Ferromagnetic superexchange in insulating Cr_{2}MoO_{6} by controlling orbital hybridization

M. Zhu, D. Do, C. R. Dela Cruz, Z. Dun, J.-G. Cheng, H. Goto, Y. Uwatoko, T. Zou, H. D. Zhou, Subhendra D. Mahanti, and X. Ke

Phys. Rev. B **92**, 094419 — Published 11 September 2015

DOI: 10.1103/PhysRevB.92.094419

Ferromagnetic superexchange in insulating Cr_2MoO_6 by controlling orbital hybridization

M. Zhu[1], D. Do[1], C.R. Dela Cruz[2], Z. Dun[3], J.-G. Cheng[4,5], H. Goto[5],Y. Uwatoko[5], T. Zou[1], H. D. Zhou[3], Subhendra. D. Mahanti[1], and X. Ke[1]

[1.] *Department of Physics and Astronomy, Michigan State University, East Lansing, MI 48824, USA.*

[2.] *Quantum Condensed Matter Division, Oak Ridge National Laboratory, Oak Ridge, TN 37831, USA*

[3.] *Department of Physics and Astronomy, University of Tennessee, Knoxville, TN 37996, USA*

[4.] *Beijing National Laboratory for Condensed Matter Physics and Institute of Physics, Chinese Academy of Sciences, Beijing 100190, China*

[5.] *Institute for Solid State Physics, University of Tokyo, 5-1-5 Kashiwanoha, Kashiwa, Chiba 277-8581, Japan*

We report the magnetic and electronic structures of an inverse-trirutile compound Cr_2MoO_6. Despite the same crystal symmetry and similar bond-lengths and bond-angles as Cr_2TeO_6, Cr_2MoO_6 possesses a magnetic structure different from that seen in Cr_2TeO_6. *Ab-initio* electronic structure calculations show that the sign and strength of the Cr-O-Cr superexchange coupling is strongly influenced by the hybridization between the filled O 2*p* and empty Mo 4*d* orbitals: the virtual transfer of an O 2*p* electron to the empty Mo 4*d* orbitals leaves the O 2*p* partially occupied, which leads to ferromagnetic exchange between Cr moments. This result further substantiates our recently proposed mechanism for tuning the exchange interaction between two magnetic atoms by modifying the electronic states of non-magnetic atoms in the exchange path through orbital hybridization. This approach is fundamentally different from the

conventional methods of controlling the exchange interaction by either carrier injection or through structural distortions.

Understanding the origin and nature of exchange interaction between the electrons in magnetic atoms has been a fundamental topic to elucidate a wide range of magnetic phenomena in condensed matter systems for many decades. For instance, the celebrated Hund's rule, which favors the electronic state with highest multiplicity, arises from the Coulomb exchange of electrons within the *d* orbitals of the same atom. In transition metal oxides, the exchange coupling between magnetic cations is prevalently mediated by the intervening non-magnetic oxygen atoms. This indirect exchange coupling, named superexchange interaction, was first studied by Kramers [1] and Anderson [2] in the framework of the perturbation theory, and the sign of the exchange integral is formulated by Goodenough-Kanamori rules based on the symmetry consideration of occupied electron orbitals [3,4]. To date, magnetic interaction is still a subtle question to investigate in real systems in spite of the great success of the direct and indirect mechanisms proposed in understanding the origin of magnetic coupling in a variety of systems. A well-known example of magnetic exchange that has attracted considerable interest in recent years is the Zener double exchange mechanism, which explains the metallicity and ferromagnetism in the mixed-valence Mn compounds [5].

The ordered inverse-trirutiles, such as Cr_2WO_6 and Cr_2TeO_6, are a series of materials in which the magnetic coupling cannot be explained only by the antiferromagnetic superexchange interaction based on the Goodenough-Kanamori rules. The space group is $P4_2/mnm$, and the bond-lengths and the bond-angles are nearly identical in both compounds [6]. However, their magnetic structures are quite distinct and the Cr-O-Cr magnetic coupling depends on whether the Te or W occupies the nonmagnetic sites [6]. Recently we presented the sign reversal of the magnetic exchange in the $Cr_2(Te_{1-x}W_x)O_6$ system at $x = 0.7$, where both the transition temperature and the average sublattice magnetic moment reach their minimum values, and we

argued that the hybridization of unoccupied W 5*d* orbitals with filled O 2*p* orbitals played an essential role in determining the nature of Cr-Cr superexchange via O 2p [7]. The competition between the usual antiferromagnetic superexchange and the ferromagnetic interaction induced by the 5*d*-2*p* hybridization could account for the sign and strength of the magnetic couplings in this system. To further substantiate the proposed orbital hybridization effect of the non-magnetic ions with empty *d*-orbitals in determining the exchange interaction, we have studied the magnetic property and the electronic structure of another inverse-trirutile Cr_2MoO_6. In this system, the presence of the low-lying unoccupied Mo 4*d* orbitals hybridizing with the occupied 2*p* orbitals of the oxygen atom in the Cr-O-Cr superexchange path should give rise to a ferromagnetic coupling between Cr-Cr atoms, as in the W compound. This is precisely what we have observed and report in this article. As we will discuss later, the physical origin of ferromagnetic exchange in Cr_2MoO_6 and also in Cr_2WO_6 differs fundamentally from the proposed antiferromagnetic exchange mechanisms via the empty Ti 3d orbitals in perovskite $EuTiO_3$ [8] and in double perovskite $CaCu_3Ti_4O_{12}$ [9].

Polycrystalline samples of Cr_2MoO_6 [10] were synthesized under high-pressure and high-temperature conditions using a cubic anvil system. The mixtures of Cr_2O_3 and MoO_3 in the stoichiometric ratio were ground thoroughly and reacted at 1000°C for 30 min under 4 GPa. Phase purity of the obtained product was first examined at room temperature with the powder X-ray diffraction. Magnetic susceptibility was measured using the Quantum Design SQUID magnetometer and specific heat was characterized using the Physical Properties Measurement System (Quantum Design). The neutron power diffraction (NPD) measurements on the sample of ~ 1g were performed on HB2A neutron powder diffractometer at High Flux Isotope Reactor (HFIR) in Oak Ridge National Laboratory. The NPD data were taken with the neutron

wavelength λ = 2.41 Å and a collimation of 12'-open-6', and were analyzed using the Rietveld refinement program FULLPROF [11].

The schematics of both crystal structure and the obtained magnetic structure of Cr_2MoO_6 are shown in Fig. 1. It has an inverse-trirutile structure with tetragonal symmetry $P4_2/mnm$, and the lattice parameters are $a = b = 4.58717(9)$ Å, and $c = 8.81138(22)$ Å at $T = 4$ K. As seen in Table 1, the Cr-O-Cr bond-angles and bond-lengths are close to those of Cr_2WO_6 and Cr_2TeO_6 due to the similar ionic radii of Mo^{6+}, Te^{6+}, and W^{6+}. As to be shown later, Cr_2MoO_6 undergoes a paramagnetic-antiferromagnetic transition at $T_N = 93$ K with the same spin order as Cr_2WO_6. One can visualize the magnetic structure in terms of each Cr^{3+} bilayer separated by a Mo layer. The Cr^{3+} spins are aligned in parallel within the *ab* plane but are antiparallel between the bilayers (Cr1-Cr3 and Cr2-Cr4). The intra-bilayer coupling between two nearest-neighbor Cr^{3+} spins (Cr1-Cr2, and Cr3-Cr4) is ferromagnetic as seen in Cr_2WO_6, in contrast to the antiferromagnetic coupling in Cr_2TeO_6 [6,7]. The close similarity in the crystal structures of these compounds with dramatically distinct magnetic structures (Cr_2MoO_6 and Cr_2WO_6 vs. Cr_2TeO_6) underscores the limitations of the Goodenough-Kanamori rules [3,4] in predicting the nature of the exchange interaction in these complex systems with competing exchange mechanisms. The role of other non-magnetic ions (e.g., Mo, W, Te) in the superexchange mechanism has to be reexamined in detail.

Figure 2 (a) shows the temperature dependence of magnetic susceptibility measured in an external field $H = 1000$ Oe. A broad peak is observed near $T_p \sim 98$ K, implying the presence of short-range antiferromagnetic correlation near and above this temperature. Inset displays the inverse susceptibility and a Curie-Weiss fit is performed in the temperature range 200 K ~ 300 K. The fitting gives a Weiss temperature $\theta_w \sim -254.4$ K and the effective magnetic moment μ_{eff} is

estimated to be 2.92 μ_B / Cr, close to the expected value 3 μ_B for the Cr^{3+} spins. The negative θ_w is consistent with the dominance of antiferromagnetic correlations in Cr1-Cr3 and Cr2-Cr4 dimers [12] in this system. The increase in the susceptibility at low temperatures is presumably due to paramagnetic impurities [7,13]. The magnetic heat capacity as a function of temperature, $C_{mag}(T)$, is shown in Fig. 2(b) with the phonon contribution subtracted by the scaled heat capacity of an isostructural non-magnetic compound Ga_2TeO_6 from the total heat capacity measured (see the inset of Fig. 2b). The sharp peak at $T_N \sim 93$ K shown in $C_{mag}(T)$ indicates a transition into a long-range ordered antiferromagnetic state. It is noteworthy that the transition temperature T_N is slightly lower than T_p determined from the broad peak in the magnetic susceptibility, which seems to be a common feature in the inverse trirutiles such as Cr_2TeO_6, Cr_2WO_6 and Fe_2TeO_6 [7,13]. Such a feature is associated with the presence of short-range low-dimensional magnetic fluctuations prior to entering a three-dimensional long-range antiferromagnetic state. The integrated magnetic entropy is shown in Fig. 2 (d) with a saturated value of 5.30 J/K mol_{Cr}, which is about 50% of the theoretical value (11.5 J/K mol_{Cr}) for spin S = 3/2 Cr^{3+} ions. The presence of resultant residual magnetic entropy implies the existence of magnetic correlation in the system above T_N. Note that residual magnetic entropy (6.20 J/K mol_{Cr}) is nearly half of the maximum value and is commonly observed in low dimensional and frustrated magnetic systems with competing interactions [14]. It has also been seen in $Cr_2(Te_{1-x}W_x)O_6$ [7], suggesting one of these factors to be present in Cr_2MoO_6 [15].

The NPD data measured at $T = 4$ K is show in Figure 3. The magnetic propagation wave vector is determined to be (0 0 1). Representational analysis using the BasIrreps program in FULLPROF [11] suggests that the magnetic structure shown in Fig. 1 is symmetry compatible and the most plausible fit to the data. The R-Bragg factors for the refinement of nuclear and

magnetic phases are 7.44 and 22.6, respectively. This magnetic structure is identical to that of Cr_2WO_6, that is, the intra-bilayer coupling (for example, Cr1-Cr2) is ferromagnetic. Note that the in-plane spin direction could not be unambiguously determined because of the tetragonal structure of the system and the nature of neutron powder data. The full width at half maximum (FWHM) of the magnetic Bragg peaks is determined by the instrumental resolution according to the refinement, confirming the long-range character of the magnetic order. Inset shows the zoom-in view of the magnetic Bragg peak Q = (0 0 1) at 4 K and 150 K. The temperature dependence of the order parameter (sublattice magnetization) is presented in Fig. 2(c), and the solid curve is a guide to the eyes. The magnetic signal disappears at the antiferromagnetic transition temperature $T_N \sim 93$ K, consistent with the specific heat measurement. Note that the magnitude of the static magnetic moment ($\approx 2.47\ \mu_B$/Cr) extracted from NPD measurement is smaller than the theoretical value of 3.0 μ_B/Cr, which is attributed to quantum spin fluctuation (at low T) as well as due to the covalence [16,17,18].

The observed ferromagnetic intra-bilayer coupling in Cr_2MoO_6 is consistent with a mechanism we proposed earlier for the W compound [7]; the nearby unoccupied Mo 4*d* orbitals (in the place of unoccupied W 5 d orbitals) plays an essential role in determining the sign of the Cr-Cr exchange by hybridizing with intervening filled O *p*-orbitals. That is, the *d*-*p* hybridization induced ferromagnetic exchange dominates the usual superexchange interaction in Cr_2MoO_6 and Cr_2WO_6. In contrast, in Cr_2TeO_6, a compound with similar crystal structure but with no empty Te *d* orbitals, the superexchange interaction between two intra-bilayer Cr moments is antiferromagnetic. However, in spite of the similarity, i.e., the presence of the empty *d* orbitals, the Neel temperature of Cr_2MoO_6 is considerably higher than that of the Cr_2WO_6, $T_N \sim 45$ K. Possible explanation of this difference will be discussed later.

To understand Cr_2MoO_6 electronic structure and its magnetic properties, we carried out first-principles calculations for four different interbilayer-intrabilayer magnetic configurations, i.e. AF-AF, AF-F, F-AF, and F-F, where AF and F denote antiferromagnetic and ferromagnetic alignments respectively. Density Functional Theory (DFT) Calculations were done within generalized gradient approximation (GGA) and GGA+U [19] as implemented in the Vienna ab-initio Simulation Package (VASP) [19,20,21], using projector-augmented wave (PAW) method [22,23] and Perdew-Burke-Ernzerhof (PBE) exchange-correlation functional [24]. The plane-wave energy cutoff and total energy accuracy are set at 400 eV and 10^{-3} eV, respectively. To sample the Brillouin zone, we use the Monkhorst-Pack schemes with the k-mesh of 14×14×7 for self-consistent calculations and 20×20×10 to get the density of states (DOS). According to the total energies of different magnetic configurations listed in Table 2, we can see that both GGA and GGA+U calculations give the ground state as AF-F, consistent with the experimental result. However, unlike Cr_2WO_6 and Cr_2TeO_6 [7], GGA gives a small negative band gap (data not shown) in Cr_2MoO_6 while the experiment shows an insulating behavior. Note that GGA usually underestimates the band gap in semiconductors [25] and the problem is severe in systems containing 3 *d*-electrons such as Cr. This problem can be partially corrected through GGA+U approximation [26,27].

Figure 4 presents the density of state (DOS) and projected DOS of Cr_2MoO_6 calculated using GGA+U with U = 4 eV for Cr. GGA+U indeed opens up a band gap and increases the Cr^{3+} magnetic moment from ~2.5 μ_B for GGA to ~2.9 μ_B for GGA+U. Reduction from 3.0 μ_B to 2.9 μ_B is due to the covalency and comparison with the experimental value, 2.47 μ_B, suggests that effect of quantum spin fluctuation is important in this system [16,17,18]. Note that in our electronic structure calculations, the principle axis is along the tetragonal axes which are not

aligned with the cubic axis of the local crystal field of the CrO_6 system, which gives rise to the mixture of both t_{2g} and e_g states in the former coordinate system for Cr 3*d* orbitals. Also note that Mo 3*d* orbitals were treated as core states and were not a part of the manifold of active orbitals because of the large energy difference (~ 235.45 eV) between O 2*p* and Mo 3*d*; therefore, the notation of d orbitals of Mo hereafter refers to its 4*d* orbitals. The projected DOS shows that there is strong hybridization between Mo-*d* and O-*p* near the bottom of the O *p*-band (-4 to -6.5 eV), and this hybridization also shows up in the lower part of the conduction band [28,29]. This strong hybridization is due to small distance between Mo and O (~ 1.9 Å). The Cr *d*-states, which are mainly in the energy range 0 to -4 eV, do not hybridize strongly with Mo d states due to large Cr-Mo distance (~ 3.0 Å and ~ 3.5 Å). However, the perturbed (by mixing with Mo *d*) O *p* bands hybridizing with the Cr *d* states (Cr-O distance is ~ 1.9 Å) lead to a ferromagnetic interaction between the intra-bilayer Cr spins. This physics is very similar to what we found in Cr_2WO_6 [7]. As elaborated in the cartoon shown in Fig. 5, a simple perturbative way of understanding this ferromagnetic coupling is that hybridization of O *p* with empty Mo *d* orbitals creates a virtual hole in the O *p*-band. This "hole" leads to a ferromagnetic coupling between two Cr^{3+} *d* spins which flank this oxygen atom. In this sense, the empty 5*d* orbitals of the Mo is responsible for the observed ferromagnetic coupling between nearest-neighbor intra-bilayer Cr spins, quite similar to what happens in the W compound.

To visualize the magnetic ordering and orbital hybridization effect, we show the spin densities projected onto the (110) plane in Figure 6. We can see that the intra-bilayer (Cr1-Cr2, Cr3-Cr4) Cr spin densities are the same (ferromagnetic ordering, blue-blue or red-red) and inter-bilayer (Cr1-Cr3, Cr2-Cr4) spin densities are opposite (antiferromagnetic ordering, red-blue), which is very similar to that of Cr_2WO_6 but in contrast to Cr_2TeO_6 [7]. The remarkable

difference is seen in the spin density associated with the oxygen atom (O2) which mediates the intra-bilayer exchange between Mo (W) and Te. In the former both lobes are of the same polarization, whereas for Te they have opposite polarization (for W and Te please see Ref.7), characteristic of ferromagnetic and antiferromagnetic coupling between Cr1 and Cr2 respectively.

We would like to note that the mechanism of the intrabilayer ferromagnetic coupling in Cr_2MoO_6 and Cr_2WO_6 via the empty 4*d* (5*d*) obitals of Mo (W) discussed above is fundamentally different from proposed antiferromagnetic exchange mechanisms in $EuTiO_3$ [8] and $CaCu_3Ti_4O_{12}$ [9] via the empty 3*d* orbitals of Ti. In $EuTiO_3$, the exchange interaction between two nearest neighbor Eu f^7 moments comes from three mechanisms [8]: (i) an antiferromagnetic superexchange through filled oxygen 2*p* states, (ii) a ferromagnetic coupling through hybridization between Eu *f* states at one site with empty Eu 5d orbitals at the other (followed by Hunds exchange coupling between Eu f and d at the same site-the well-known Kasuya mechanism [30]), and (iii) an antiferromagnetic superexchange through empty Ti 3*d* orbitals. (i) is quite small and (ii) and (iii) compete. Small changes in the lattice constant (introduced by strain) can tune this competition and change the nearest neighbor Eu-Eu interaction from antiferro- to ferromagnetic [31]. In principle the ferromagnetic exchange coupling proposed by us could also be present in $EuTiO_3$. The empty Ti 3d orbitals can hybridize with O p which mediates the superexchange between two Eu moments. However, in this compound the Eu-O-Eu superexchange is extremely small (zero) due to 90^o superexchange path (Eu-O-Eu bond angle). Thus the mixing of O p with Ti d does not do much to this very small superexchange. In $CaCu_3Ti_4O_{12}$, Toyoda et al [9] found that the long range exchange interaction (third nearest neighbor) between two Cu moments is mediated through two O and one Ti atom in a Cu-O-Ti-O-Cu exchange path where the empty 3 *d* orbitals of Ti introduces an

antiferromagnetic exchange between two Cu moments. A similar physics also operates when Ti is replaced by Zr, the empty 4*d* orbitals of the Zr atom playing the role of Ti 3*d* orbital.

Finally, we would like to comment the difference in T_N of Cr_2MoO_6 and Cr_2WO_6. For this purpose, we have calculated the sign and the strength of the inter-bilayer (J, Cr3-Cr1 distance ~ 2.780 Å) and intra-bilayer (j, Cr3-Cr4 distance ~ 3.626 Å) exchange interaction between Cr moments using a simple nearest neighbor Heisenberg model $H = -2\sum_{<ij>} J_{ij}\vec{S}_i \cdot \vec{S}_j$ for the two compounds within GGA and GGA+U. The respective values are given in the Table 3. Note that compared to J and j, further neighbor interactions (e.g., the interaction between two nearest-neighbor Cr3 ions within the layer separated by a distance of 4.587 Å) is much smaller and thus negligible. A similar approximation was previously made in Ref. [12]. As seen in the table, introduction of U reduces the strengths of the exchange couplings in general. However, because of the competition between ferromagnetic and antiferromagnetic contributions to a given exchange parameter, the introduction of U affects J and j differently, not only for a given system but also between different systems. The precise quantitative values should not be taken seriously but the qualitative trends are consistent with experiment. Nevertheless, one can see that GGA+U seems to give a better description of the observed antiferromagnetic transition temperature T_N (45 K and 93 K for W and Mo compounds respectively) since the energy scale of T_N is primarily set by J. In addition, the smaller j value of Cr_2MoO_6 given by GGA+U calculation than that of Cr_2WO_6 is also consistent with the scenario that Mo 4*d* orbital is less extended than the W 5*d* one which is expected to contribute to the weaker ferromagnetic interaction induced via a lesser extent of the *d-p* orbital hybridization. More careful calculations of the total energy using improved approximations to exchange-correlation potential within DFT (both local and non-local) are needed to pin down the parameters of the exchange Hamiltonian. Also magnon dispersion

measurements and theoretical calculations will help us understand the nature of magnetic exchange in these interesting systems.

In summary, we have studied the magnetic and electronic properties of an inverse-trirutile compound Cr_2MoO_6 to examine the idea that low-lying empty *d* bands associated with Mo can induce a ferromagnetic coupling between two Cr moments by perturbing the *p* orbitals of the O atom which mediates the exchange between these two Cr atoms. The underlying physics is similar to the one we have previously suggested for Cr_2WO_6 with low lying empty W5*d* bands. GGA+U appears to give a better description of the system. However, for a quantitative understanding of the exchange parameters more theoretical work is necessary. And inelastic scattering measurement of magnon spectra will be helpful in pinning down the exchange parameters to validate the theoretical predictions.

X.K. acknowledges the support from the start-up funds at Michigan State University. D.D and S.M. acknowledge support by the Institution for Cyber Enabled Research (ICER), and High Performance Computer Center (HPCC) at Michigan State University. Z.D. and H. D. Z. thank for the support for the support of NSF-DMR-1350002. J.G.C. acknowledges the support of the NSF and MOST of China (Grant Nos. 11304371 and 2014CB921500) and the Strategic Priority Research Program of the Chinese Academy of Sciences (Grant No. XDB07020100). Work at ORNL was supported by the Scientific User Facilities Division, Office of Basic Energy Sciences, DOE.

Figure Captions

Figure 1. The schematics of the crystal and magnetic structure of Cr_2MoO_6. The Cr^{3+} spins are parallel within the *ab* plane. The intra-bilayer (Cr1-Cr2) coupling is ferromagnetic while the inter-bilayer one (Cr2-Cr3) is antiferromagnetic.

Figure 2. (a) Temperature dependence of the magnetic susceptibility. Inset shows the inverse susceptibility and the Curie-Weiss fit. (b) Temperature dependence of the magnetic heat capacity. Inset shows the subtraction of the phonon contribution using the scaled heat capacity of Ga_2TeO_6. (c) Intensity of the (0 0 1) magnetic Bragg peak as a function of temperature. The solid line is a guide to eyes. (d) Temperature dependence of the integrated magnetic entropy. The horizontal red line denotes the theoretical value for S=3/2.

Figure 3. Neutron powder diffraction data of Cr_2MoO_6 at T = 4 K. The black symbols are experimental data and the red curve is Rietveld refinement fit. The difference is represented by the blue. The positions of the nuclear and magnetic peaks are marked by the green and magenta lines, respectively. Inset shows the difference between low and high temperature data with the positions of magnetic Bragg peaks denoted by the symbol *.

Figure 4. Density of state (DOS) in the units of (# of states / (eV u.c.)) and projected density of states (PDOS) in the units of (# of states / (eV atom)) of Cr_2MoO_6 calculated by GGA+U.

Figure 5. A cartoon illustrating the ferromagnetic coupling between two Cr 3*d* moments via the orbital hybridization between O 2*p* orbitals and Mo empty 4*d* orbitals leading to a virtual electron transfer from O 2*p* to Mo 4*d*, leaving O 2*p* partially occupied which induces a ferromagnetic coupling between two Cr moments via Cr 3*d* - O 2*p* hybridization.

Figure 6. Spin density projected on (110) of Cr_2MoO_6 calculated using GGA+U where red and blue indicate spin up and down, respectively. Similar results for the W and Te compounds are given (from Ref. **7**). Since the local cubic axes of the CrO_6 octahedra are rotated from the chosen tetragonal x-y-z coordinates (see Fig.1), in the latter coordinate system Cr *d*-t_{2g} and *d*-e_g states are mixed.

Table 1. Structural parameters ($T = 4$ K) of Cr_2TeO_6, Cr_2WO_6, and Cr_2MoO_6, including lattice parameters, bond length, and bond angles.

Compound		Cr_2TeO_6	Cr_2WO_6	Cr_2MoO_6
Lattice Parameters (Å)	a	4.54487(8)	4.58346(5)	4.58717(9)
	b	4.54487(8)	4.58346(5)	4.58717(9)
	c	8.99539(21)	8.85319(13)	8.81138(22)
Bond Length (Å)	Cr3-Cr1	2.968(14)	2.930(13)	2.78(3)
	Cr3-Cr4	3.559(7)	3.558(6)	3.603(8)
	Cr3-Cr3	4.54487(8)	4.58346(5)	4.58717(9)
Bond Angle (degree)	Cr3-O1-Cr1	98.5(3)	97.6(3)	96.65(16)
	Cr3-O2-Cr4	127.0(4)	128.6(3)	130.3(3)

Table 2. Total energies (in eV) per magnetic unit cell containing four Cr^{3+} ions of different magnetic configurations.

Configuration	AF-AF	AF-F	F-AF	F-F
GGA	-153.325	**-153.520**	-153.457	-153.422
GGA+U	-143.649	**-143.671**	-143.562	-143.635

Table 3. Exchange parameters J and j obtained from the simple isotropic Heisenberg model $H = -2\sum_{<ij>} J_{ij}\vec{S}_i \cdot \vec{S}_j$; $J_{ij} = j$ for nearest neighbor (nn) intra-bilayer and $J_{ij} = J$ for nn inter-bilayer exchange. Values with superscript * are obtained using GGA based on a model proposed in Ref. [12].

Compound	Cr_2MoO_6		Cr_2WO_6	
Parameter	J (meV)	j (meV)	J (meV)	j (meV)
Theo. (GGA)	-5.4	2.7	-10.4	1.0
Theo.(GGA+U)	-1.9	0.15	-1.0	0.75
Ref. 12			-3.8*	0.12*

Figure 1

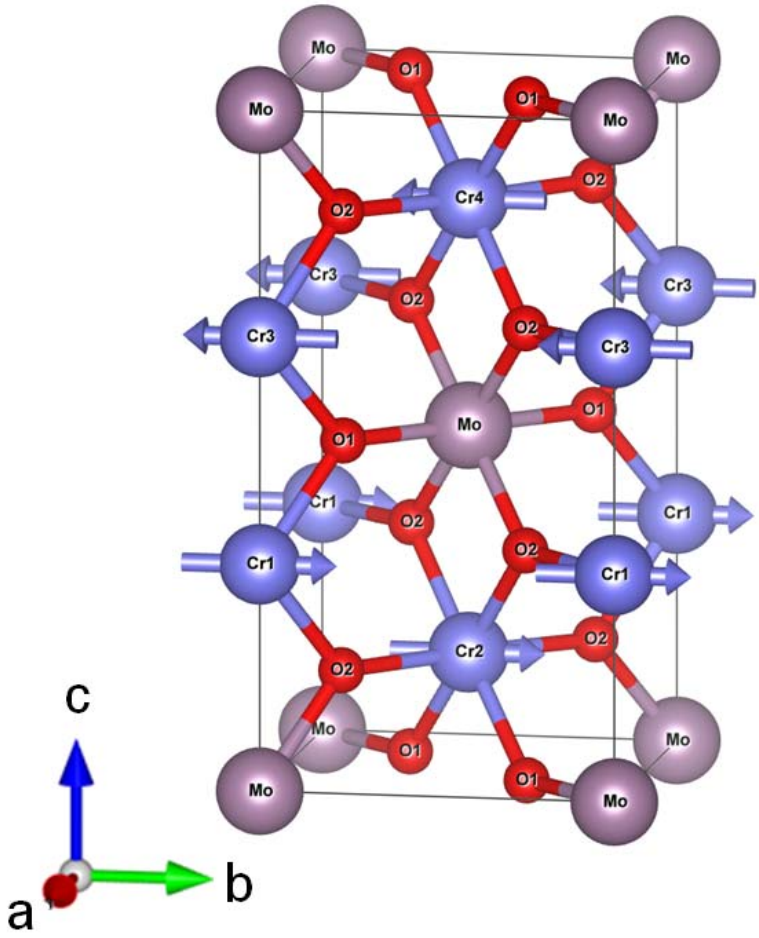

Figure 2

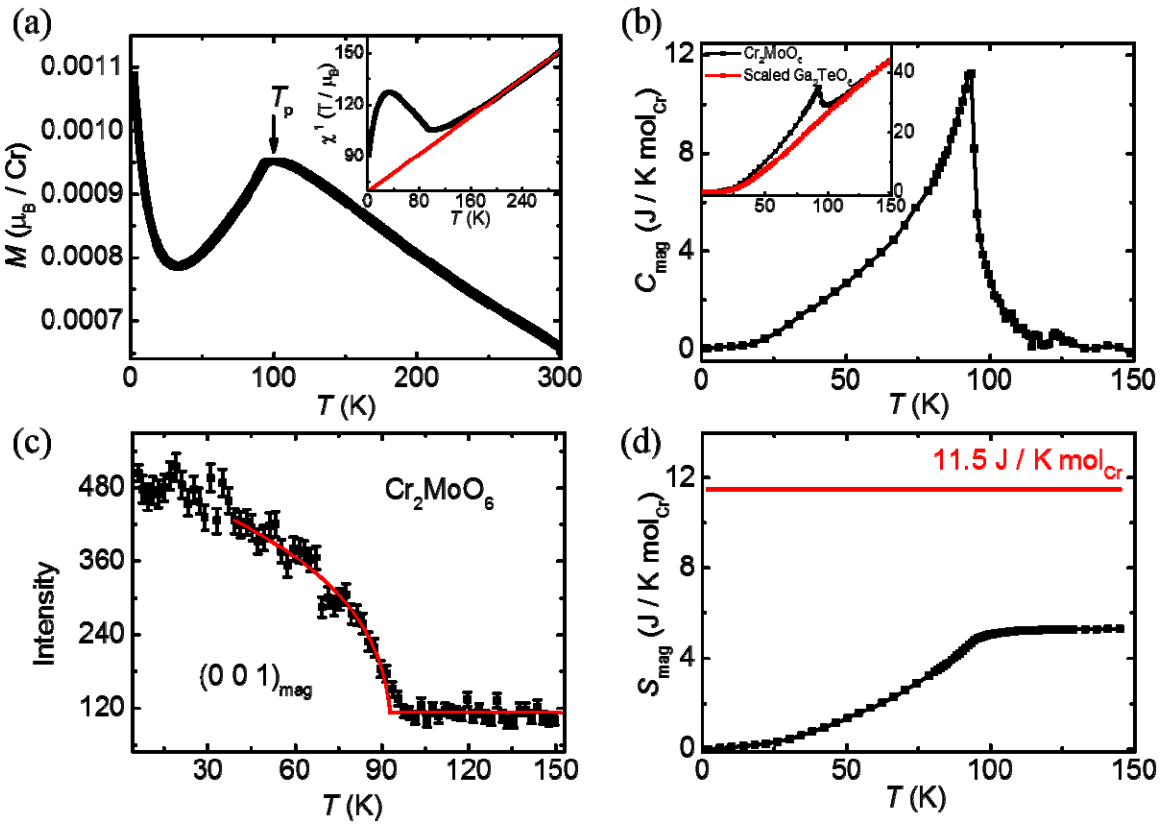
(a)
0.0011
0.0010
0.0009
0.0008
0.0007
M (μB / Cr)
Tp
0
100
200
300
T (K)
150
120
90
χ-1 (T / μB)
0
80
160
240
T (K)
(b)
12
8
4
0
Cmag (J / K molCr)
Cr2MoO6
Scaled Ga2TeO6
40
20
0
50
100
150
0
50
100
150
T (K)
(c)
480
360
240
120
Intensity
Cr2MoO6
(0 0 1)mag
30
60
90
120
150
T (K)
(d)
12
8
4
0
Smag (J / K molCr)
11.5 J / K molCr
0
50
100
150
T (K)

Figure 3

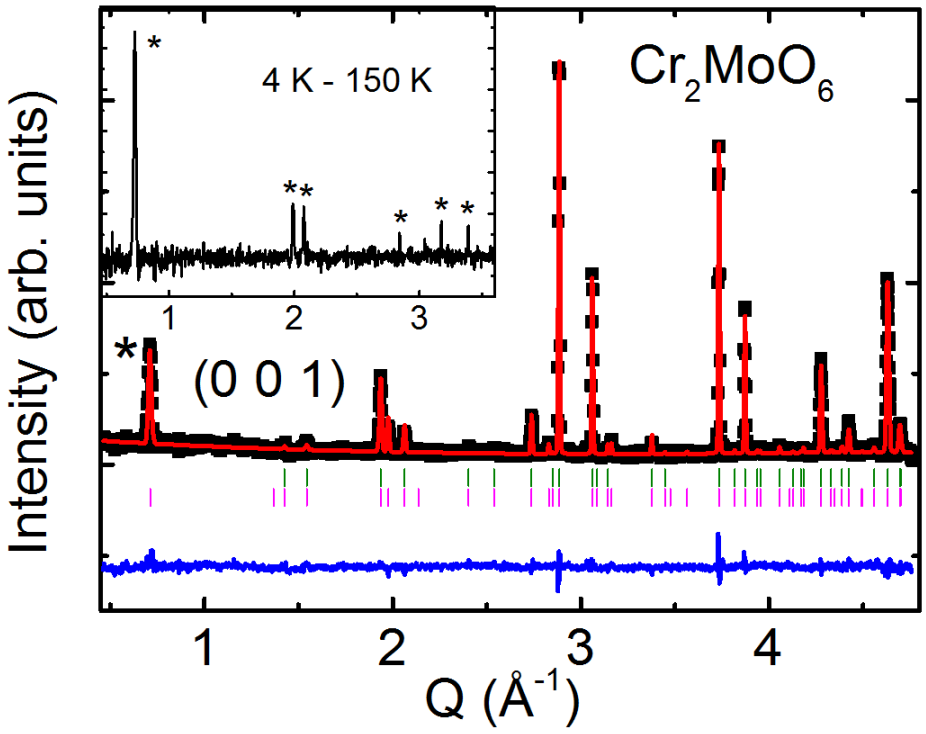

Figure 4.

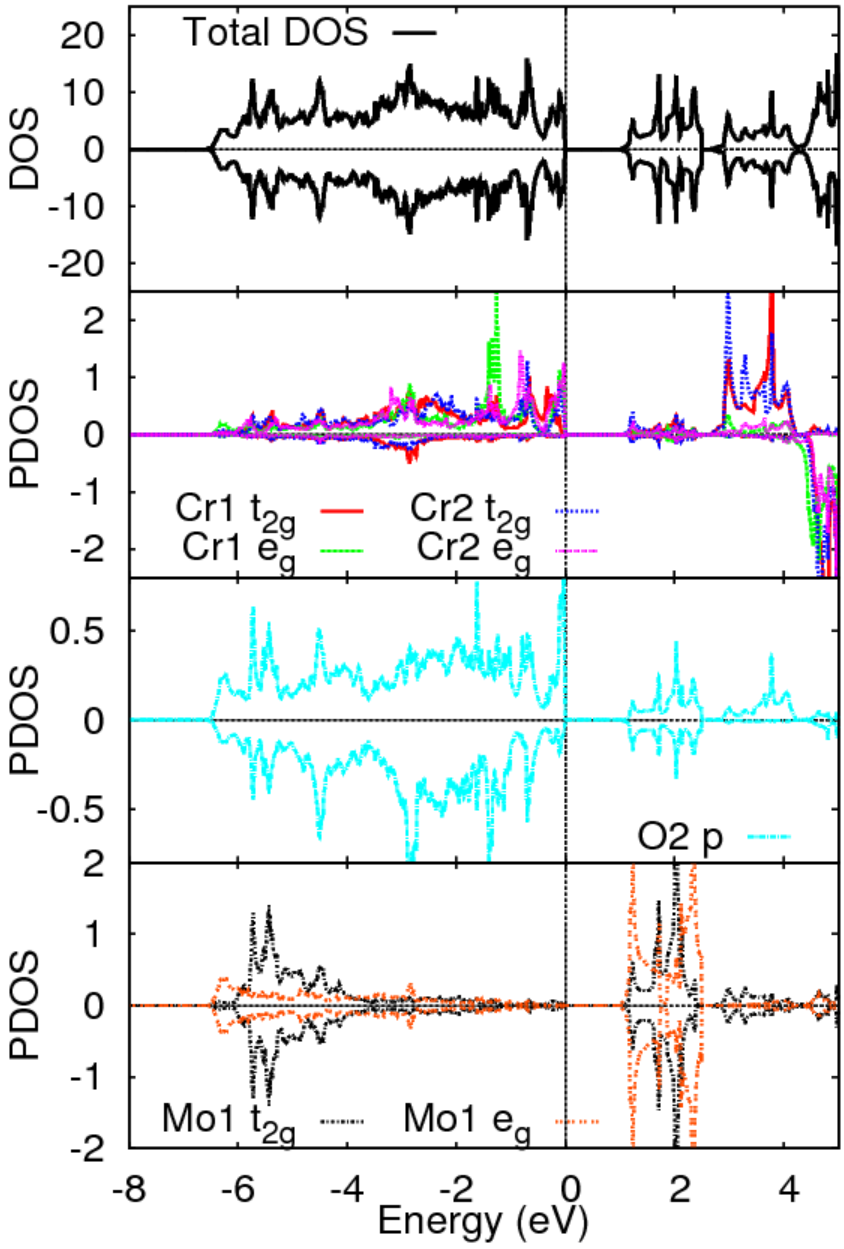
Total DOS
DOS
PDOS
Cr1 t_{2g}
Cr1 e_g
Cr2 t_{2g}
Cr2 e_g
O2 p
Mo1 t_{2g}
Mo1 e_g
Energy (eV)

Figure 5.

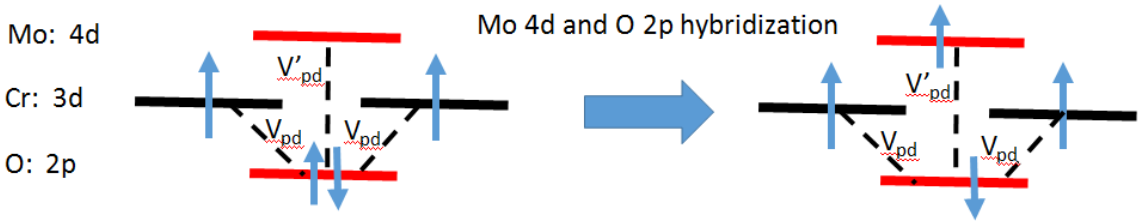
Mo: 4d
Cr: 3d
O: 2p
V'pd
Vpd
Vpd
Mo 4d and O 2p hybridization
V'pd
Vpd
Vpd

Figure 6

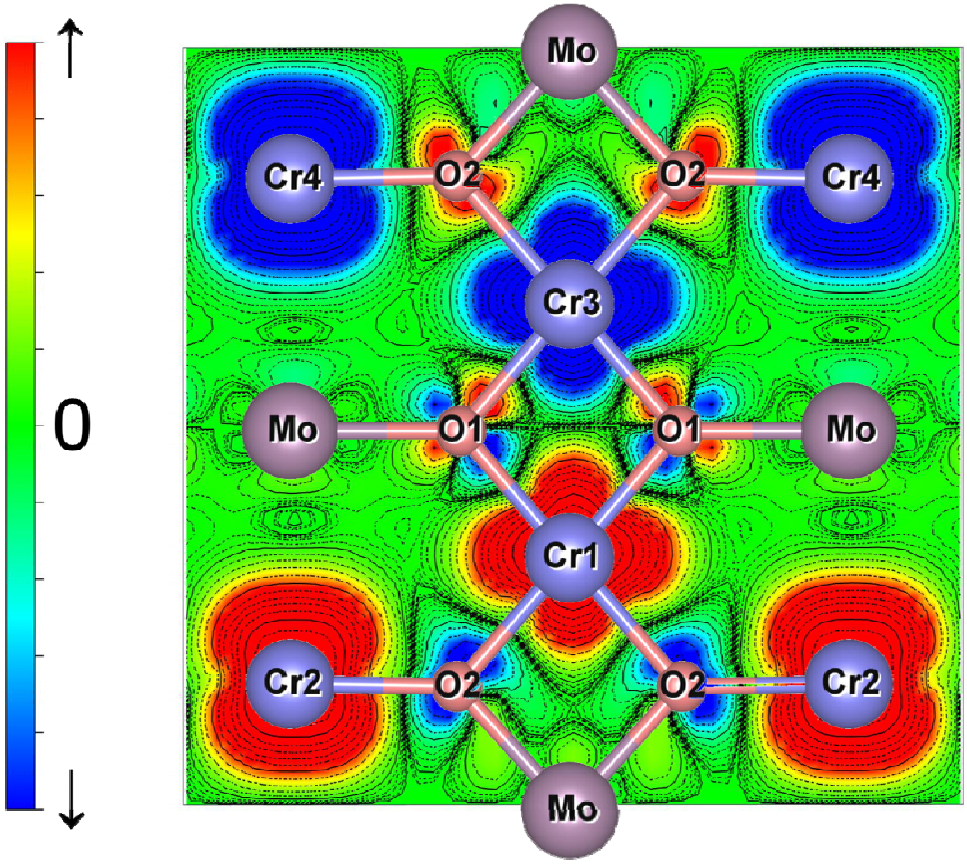

[1] H. A. Kramers, Physica **1**, 182 (1934).

[2] P. W. Anderson, Phys. Rev. **79**, 350 (1950).

[3] J. Kanamori, J. Phys. Chem, Solids **10**, 87 (1959).

[4] J. B. Goodenough, Phys. Rev. **100**, 564 (1955).

[5] C. Zener, Phys. Rev. **82**, 403 (1951).

[6] W. Kunnmann, S. La Placa, L. M. Corliss, J. M. Hastings and E. Banks, J. Phys. Chem. Solids **29**, 1359 (1968).

[7] M. Zhu, D. Do, C. R. Dela Cruz, Z. Dun, H. D. Zhou, S. D. Mahanti and X. Ke, Phys. Rev. Lett. **113**, 076406 (2014).

[8] H. Akamatsu, Y. Kumagai, F. Oba, K. Fujita, H. Murakami, K. Tanaka, and I. Tanaka, Phys. Rev. B 83, 214421 (2011).

[9] M. Toyoda, K. Yamauchi, and T. Oguchi, Phys. Rev. B 87, 224430 (2013).

[10] A. Collomb, J. J. Capponi, M. Gondrand, J. C. Joubert, J. Solid State Chem. **23**, 315 (1978)

[11] J. Rodríguez-Carvajal, Physica (Amsterdam) 192B, 55 (1993).

[12] M. Drillon, L. Padel, and J. C. Bernier, Physica (Amsterdam) 97B+C, 380 (1979);

[13] M. Yamaguchi and M. Ishikawa, J. Phys. Soc. Jpn **63**, 1666 (1994).

[14] R. Moessner and A. P. Ramirez, Phys. Today, Feb. (2006) P24.

[15] Since the strongest exchange interaction is between the two Cr^{3+} moments forming dimers Cr1-Cr3, it is possible that above T_N intra-dimer spin correlations still persist which will lead to a reduction in the magnetic entropy from the free ion (S=3/2) value.

[16] P. J. Brown, J. B. Forsyth, E. Lelièvre-Berna, and F. Tasser, J. Phys. Condens. Mater. **14**, 1957 (2002).

[17] S. D. Mahanti and T. A. Kaplan, J. Appl. Phys. **69**, 5382 (1991).

[18] T. A. Kaplan. S. D. Mahanti, and H. Chang, Physical Review B **45**, 2565 (1992).

[19] S. L. Dudarev, G. A. Botton, S. Y. Savrasov, C. J. Humphreys, and A. P. Sutton, Physical Review B **57** (3), 1505 (1998).

[20] G. Kresse and J. Furthmüller, Computational Materials Science **6** (1), 15 (1996).

[21] G. Kresse and J. Furthmüller, Physical Review B **54** (16), 11169 (1996).

[22] G. Kresse and J. Hafner, Physical Review B **47** (1), 558 (1993).

[23] G. Kresse and D. Joubert, Physical Review B **59** (3), 1758 (1999).

[24] John P. Perdew, Kieron Burke, and Matthias Ernzerhof, Physical Review Letters **77** (18), 3865 (1996).

[25] R.M. Martin, *Electronic Structure Theory: Basic Theory and Practical Methods* (Cambridge University Press, Cambridge, UK, 2004).

[26] Vladimir I. Anisimov, Jan Zaanen, and Ole K. Andersen, Physical Review B **44** (3), 943 (1991).

[27] V. I. Anisimov, I. V. Solovyev, M. A. Korotin, M. T. Czyżyk, and G. A. Sawatzky, Physical Review B **48** (23), 16929 (1993).

[28] The dominant mixing between O 2p and Mo d orbitals comes from the latter's 4d orbitals, not from the deep lying 3d orbitals. This is easily seen by looking at the atomic energies of O 2p (E_{O2p} = - 0.632 au), Mo 4d (E_{Mo4d} = -0.358 au) and Mo 3d (E_{Mo3d} =-9.284 au). The energy difference between O 2p and Mo 4d is ~7.45 eV whereas that between O 2p and Mo 3d is ~235.45 eV. Thus O 2p and Mo 3d mixing is expected to be extremely small. In fact in our electronic structure calculations Mo 3d were treated as core state and not a part of the manifold of active orbitals. In a recent paper on α-MoO3 [29], the authors stated that the hybridization of

O 2p is with Mo 3d. This is just a mistake because they use the same electronic structure package that we have used and the Mo 3d states are treated as core states).

[29] P.R. Huang, Y. He, C. Cao, and Z. H. Lu, Sci. Rep. **4**: 7131, (2014).

[30] T. Kasuya, IBM J. Res. Dev. **14**, 214 (1970).

[31] C. J. Fennie and K. M. Rabe, Phys. Rev. Lett. **97**, 267702, (2006).